J. Phys. B: At. Mol. Opt. Phys. **32** (1999) 3965–3972. Printed in the UK PII: S0953-4075(99)03689-5

The orientational dichroism in (e, 2e) collisions: interplay between geometrical and dynamical effects

J Berakdar† and S Mazevet‡

† Max-Planck Institut für Mikrostrukturphysik, Weinberg 2, 06120 Halle, Germany
‡ Department of Physics and Astronomy, 440 W Brooks, Norman, OK 73019, USA

Received 23 April 1999, in final form 11 June 1999

Abstract. The fully differential cross sections for the electron-impact ionization of atomic targets, prepared in a given circular state using laser-pumping, reveal a dependence on the inversion of the helicity of the exciting photon. This 'dichroism' effect was shown to be strongly dependent on the geometrical arrangements of the experiment both theoretically and experimentally. In addition, as shown theoretically in this paper, the dichroism may also vanish at certain 'non-geometrical' points that can be deduced analytically within the first Born approximation. More elaborate calculations using the distorted-wave Born approximation confirm this analysis. On the basis of this study, we further suggest a possible explanation for a structure observed recently in the state-resolved fully differential cross sections for a sodium target.

A typical (e, 2e) experiment measures the cross section for the single ionization of a target in its ground state following the impact of an electron beam of well defined momentum $\boldsymbol{p}_0$. The experimental set-up simultaneously resolves the vector momenta $\boldsymbol{p}_a$ and $\boldsymbol{p}_b$ of the two receding electrons, the scattered and the electron ejected from the target, i.e. the energies and emission angles of these two electrons are determined in coincidence. Depending upon the kinematical conditions of the experiment, various types of information can be extracted from the (e, 2e) signal. For example, under favourable situations, the (e, 2e) technique has been exploited to study the target's electronic structure (McCarthy and Weigold 1976), final-state interactions (Ehrhardt *et al* 1997) as well as spin effects (Baum *et al* 1992, Guo *et al* 1996, Dorn *et al* 1997, Prinz *et al* 1996).

One relatively recent facet of the (e, 2e) reaction is the dependence of the fully differential cross section on the initial orientation of the atomic target. This dependence, termed *orientational dichroism*, implies that the initial orientation of the bound atomic electron is transferred dynamically to the *two* outgoing continuum electrons. Experimentally, the initial-state orientation is achieved by optical pumping of the atomic targets with a laser of a given circular polarization. The information that such an experiment yields has been expressed in terms of an irreducible set of tensorial parameters whose number is determined by the symmetry of the initially prepared target state (Berakdar *et al* 1996). The tensorial parameter that quantifies the orientational dichroism for a P state is a vector. Its component (along the quantization axis of the target) $\Lambda_0^{(1)}$ is given by (the $\boldsymbol{L}\cdot\boldsymbol{S}$ interaction is neglected)

$$\Lambda_0^{(1)} = \frac{1}{\sqrt{2}}(\sigma_{1,1} - \sigma_{1,-1}). \tag{1}$$

0953-4075/99/153965+08$30.00

The cross sections σ_{L,m_L} for the ionization of an atomic target in a quantum state of orbital angular momentum L and magnetic quantum number m_L are given by

$$\sigma_{L,m_L} = C\ |T_{L,m_L}|^2, \tag{2}$$

where the kinematical factor C has the value $C = (2\pi)^4 p_a p_b / p_0$. The transition matrix elements T_{L,m_L} are given by

$$T_{L,m_L} = \langle \psi_{\boldsymbol{p}_a,\boldsymbol{p}_b} | V | \varphi_{\boldsymbol{p}_0;L,m_L} \rangle. \tag{3}$$

The vector $|\varphi_{\boldsymbol{p}_0;L,m_L}\rangle$ represents the initial state as prepared by the pumping process whereas $\langle \psi_{\boldsymbol{p}_a,\boldsymbol{p}_b}|$ describes the two electrons receding from the residual ion. The interaction potential, due to which this transition occurs, is referred to as V. At relatively high energies and small momentum transfer it has been shown that the first Born approximation (FBA) for $\langle \psi_{\boldsymbol{p}_a,\boldsymbol{p}_b}|$ yields a reasonable description of σ_{L,m_L} and $\Lambda_0^{(1)}$ as compared with the experiments performed on a Na target (Dorn *et al* 1998). Thus it seems worthwhile to analyse the dichroism within the FBA and compare then with more elaborate methods, in our case the distorted-wave Born approximation (DWBA).

First we perform the analysis for a hydrogenic target in the 2p state and write the state-resolved cross sections, σ_{L,m_L}, in the form

$$\sigma^{FBA}_{L,m_L} = C' T_{L,m_L} T^*_{L,m_L} \tag{4}$$

where $C' = 4p_a p_b/(p_0 q^4)$ and $\boldsymbol{q} = \boldsymbol{p}_0 - \boldsymbol{p}_a$ is the momentum transfer vector. From a lengthy but otherwise straightforward analysis the expression (4) reduces to (Fehr *et al* 1994)

$$T_{L=1,m_L=+1} = f\,\hat{\boldsymbol{\epsilon}} \cdot [a\boldsymbol{q} + b\boldsymbol{p}_b] \tag{5}$$

where $\hat{\boldsymbol{\epsilon}}$ is the polarization vector of the pumping light. The transition amplitude $T_{L=1,m_L=-1}$ is obtained from equation (5) by replacing $\hat{\boldsymbol{\epsilon}}$ by $\hat{\boldsymbol{\epsilon}}^*$. Furthermore, we introduced the quantities

$$\begin{aligned} f &= \left(\sqrt{2\pi}\, p_b^2\right)^{-1} Z^{\mathrm{i}\alpha-2} N^{-\mathrm{i}\alpha-3}, \\ Z &= q^2 - (p_b + \mathrm{i}/2)^2, \\ N &= (\boldsymbol{q} - \boldsymbol{p}_b)^2 + \tfrac{1}{4}. \end{aligned} \tag{6}$$

The Sommerfeld parameter α is given by $\alpha = -1/p_b$. The functions a and b read

$$\begin{aligned} a &= -(p_b+1)(p_b+\mathrm{i}/2)N^2 - (p_b^2+1)ZN + (\mathrm{i}-p_b)(\mathrm{i}/2-p_b)Z^2, \\ b &= (p_b-\mathrm{i})(p_b+\mathrm{i}/2)ZN + (p_b-\mathrm{i})(p_b-\mathrm{i}/2)Z^2. \end{aligned} \tag{7}$$

If we define the complex vector $\boldsymbol{A}$ as $\boldsymbol{A} := a\boldsymbol{q} + b\boldsymbol{p}_b$ we can write the cross section as

$$\sigma_{L,m_L} = C' |f|^2 (\hat{\boldsymbol{\epsilon}} \cdot \boldsymbol{A})(\hat{\boldsymbol{\epsilon}}^* \cdot \boldsymbol{A}^*). \tag{8}$$

The quantities in equation (8) that are important for the dichroism must be sensitive to inversion of the laser polarization ($\hat{\epsilon} \leftrightarrow \hat{\boldsymbol{\epsilon}}^*$). Therefore, we recouple the expression (8) in the form

$$\sigma^{FBA}_{1,m_L=+1} = C' |f|^2 [\tfrac{1}{3}(\hat{\boldsymbol{\epsilon}} \cdot \hat{\boldsymbol{\epsilon}}^*)(\boldsymbol{A} \cdot \boldsymbol{A}^*) + \tfrac{1}{2}(\hat{\boldsymbol{\epsilon}} \times \hat{\boldsymbol{\epsilon}}^*)(\boldsymbol{A} \times \boldsymbol{A}^*) + T_2(\hat{\boldsymbol{\epsilon}}, \hat{\boldsymbol{\epsilon}}^*) T_2(\boldsymbol{A}, \boldsymbol{A}^*)] \tag{9}$$

where $T_2(\boldsymbol{i}, \boldsymbol{j})$ is a tensor of rank two constructed from the spherical vectors $\boldsymbol{i}$ and $\boldsymbol{j}$.

Only the second term in relation (9) is sensitive to the replacement $m_L = +1$ by $m_L = -1$; this amounts to $\hat{\boldsymbol{\epsilon}} \leftrightarrow \hat{\boldsymbol{\epsilon}}^*$. Hence we deduce

$$\begin{aligned} \Lambda_0^{(1)} &= \frac{1}{\sqrt{2}} (\sigma^{FBA}_{1,m_L=+1} - \sigma^{FBA}_{1,m_L=-1}) \\ &= \frac{C'}{\sqrt{2}} |f|^2 (\hat{\boldsymbol{\epsilon}} \times \hat{\boldsymbol{\epsilon}}^*)(\boldsymbol{A} \times \boldsymbol{A}^*) \\ &= -\mathrm{i} \frac{C'}{\sqrt{2}} |f|^2 (ab^* - ba^*) \boldsymbol{p} \cdot (\boldsymbol{q} \times \boldsymbol{p}_b) \\ &= -\mathrm{i} C' \sqrt{2} |f|^2 \mathrm{Im}\,(ab^*) \boldsymbol{p} \cdot (\boldsymbol{q} \times \boldsymbol{p}_b). \end{aligned} \tag{10}$$

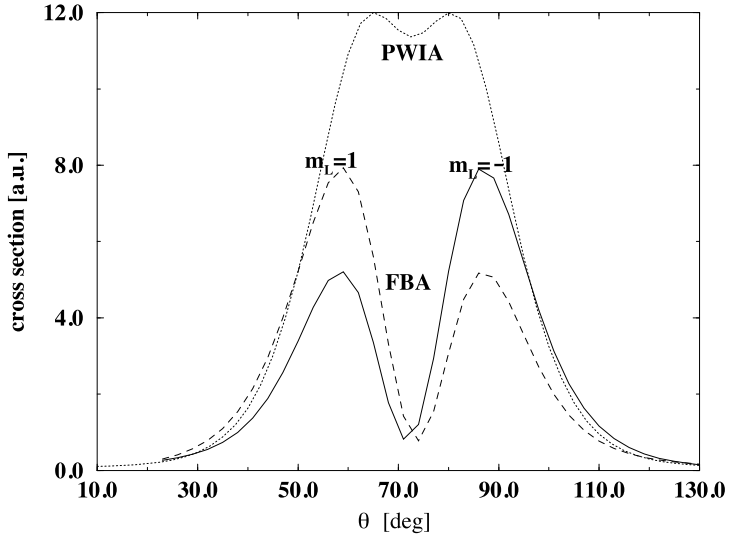

Figure 1. The state-resolved cross sections $\sigma_{L=1,m_L=\pm1}$ for the ionization of atomic hydrogen. The x-axis is chosen as the wavevector of the pumping laser whereas the incoming beam defines the z-direction. The polar angle of the scattered electron is fixed to $\theta_a = 18^\circ$ whereas the polar angle of the ejected electron θ_b is varied. The azimuthal angles are $\varphi_a = 180^\circ$ and $\varphi_b = 0^\circ$. The impact energy and the energy of the ejected electron are, respectively, $E_0 = 150$ eV and $E_b = 10$ eV. The cross sections $\sigma_{L=1,m_L=\pm1}$ are calculated within the PWIA (dotted curve) and FBA (the solid curve represents $\sigma_{1,-1}$ and the dashed curve shows the cross section $\sigma_{1,+1}$).

Here $\boldsymbol{p}$ is the wavevector of the laser light. As is clear from equation (10) the geometrical properties of $\Lambda_0^{(1)}$ are dictated by the triple product $\boldsymbol{p} \cdot (\boldsymbol{q} \times \boldsymbol{p}_b)$: the dichroism vanishes when the three vectors $\boldsymbol{p}$, $\boldsymbol{q}$ and $\boldsymbol{p}_b$ are linearly dependent. The experimental set-up can be tuned to these 'geometrical points' where $\boldsymbol{p} \cdot (\boldsymbol{q} \times \boldsymbol{p}_b) = 0$, as demonstrated experimentally by Dorn *et al* (1998). In addition, if we choose as a reference axis the direction $\boldsymbol{q}$, the functional dependence of $\Lambda_0^{(1)}$ on $\theta_b = \cos^{-1}(\hat{\boldsymbol{q}} \cdot \hat{\boldsymbol{p}}_b)$ exibits a reflection antisymmetry (with respect to $\boldsymbol{q}$) due to the vector product in equation (10). This symmetry property was also revealed by the experiment of Dorn *et al* (1998) for moderate incident energies (150 eV on a Na target) and a small momentum transfer (cf figure 4). We mention, however, that a considerable symmetry break has been observed, when the incident energy is lowered from 150 eV to 60 eV. This is a signature of the limited region of validity of the FBA, as mentioned above.

Relation (10) suggests that the dichroism may also vanish upon the *dynamical* condition Im $(ab^*) = 0$. This is, for example, the situation when $\alpha \equiv 0$ in which case the FBA reduces to the plane-wave impulse approximation (PWIA). More interestingly, for a finite α it turned out that for a given $\boldsymbol{p}_0$, $\boldsymbol{q}$ and p_b the function Im $(ab^*)(\boldsymbol{q}, p_b, \theta_b)$ vanishes *for all* θ_b. In addition, the sign of the function Im $(ab^*)(\boldsymbol{q}, p_b, \theta_b)$ is dependent on the specific values of $\boldsymbol{q}$, p_b and θ_b. Thus, the sign of the dichroism is not only determined by the triple product in equation (10) but also by the sign of Im $(ab^*)(\boldsymbol{q}, p_b, \theta_b)$. These findings are readily deduced by an analytical analysis of equation (7). However, the final result for the condition Im $(ab^*)(\boldsymbol{q}, p_b, \theta_b) = 0$, $\forall\, \theta_b$ is rather complicated. Therefore, we illustrate the results in figures 1–4.

As seen in figure 1, $\Lambda_0^{(1)}$ vanishes at $\theta_b \approx 72^\circ$ in which case $\boldsymbol{q} \parallel \boldsymbol{p}_b$. As follows from equation (10), $\Lambda_0^{(1)}(\theta_b)$ shows a reflection antisymmetry with respect to $\boldsymbol{q} \parallel \boldsymbol{p}_b$. The cross sections $\sigma_{m_L=\pm1}$ show a double-peak shape. One might think of associating this shape with the nodal structure of the bound state, as discussed by Berakdar *et al* (1996). However, as deduced

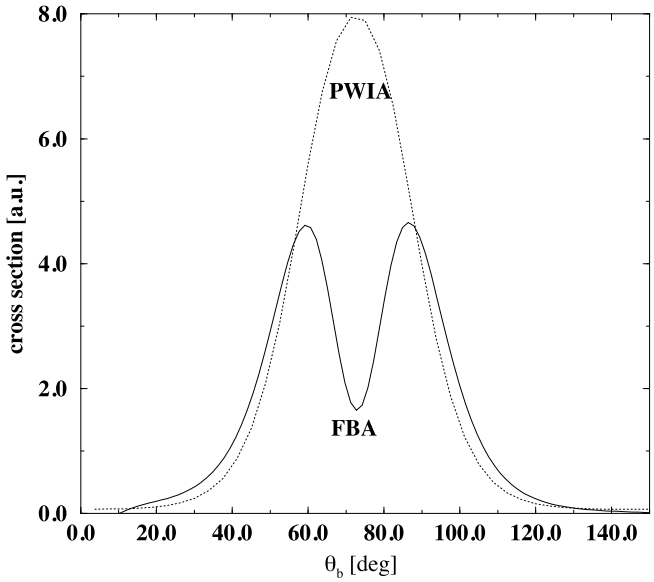

Figure 2. Same as in figure 1 and the same target but for a scattering angle $\theta_a = 19.9^\circ$. The dichroism vanishes. Hence, the cross sections $\sigma_{1,-1}$ and $\sigma_{1,+1}$ are identical.

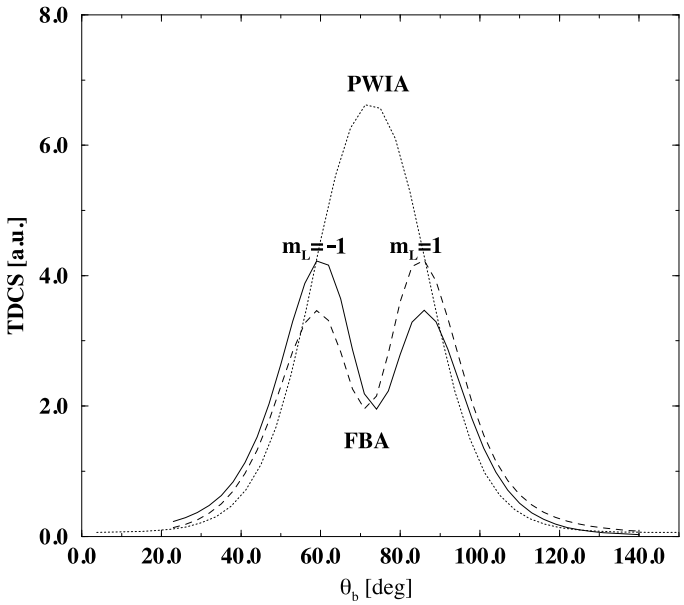

Figure 3. Same geometry and target as in figure 1 but for a scattering angle $\theta_a = 20.4^\circ$.

from figures 1–3, this impression is illusory. If the scattering angle of the fixed electron is changed slightly from $\theta_a = 18^\circ$ to $\theta_a = 19.9^\circ$ in figure 2 the dichroism disappears, since in this particular case Im $(ab^*)(\boldsymbol{q}, p_b, \theta_b) = 0\,\forall\,\theta_b$ (note that the triple product in equation (10) is virtually unchanged in the scattering geometry of figures 1 and 2). Moreover, the double-peak structure is retained whereas the PWIA shows no such structure. When further changing the

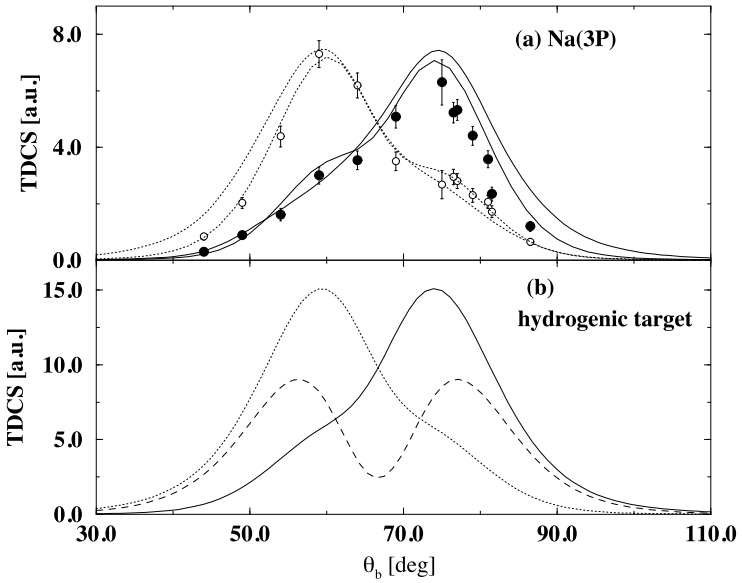

Figure 4. The same scattering geometry as in figure 1. However, the ejected electron energy is chosen as $E_b = 20$ eV and the scattering angle is fixed at $\theta_a = 20^\circ$. In (*a*) the cross section within the FBA (thin curve) and DWBA (thick curve) are shown for a Na(3P) target ($\sigma_{L=1,m_L=-1}$ (solid curve); $\sigma_{L=1,m_L=1}$ (dotted curve)). Experimental data are from Dorn *et al* (1998). (*b*) Hydrogenic target: FBA($m_L = -1$) (solid curve), FBA($m_L = 1$) (short-dashed curve) and PWIA (dashed curve).

scattering geometry from figure 2 to figure 3 the dichroism changes sign in accord with the analytical predictions. The double-peak structure is inherent to the FBA and hence to the final-state interaction of the slow electron with the residual ion. When this interaction is decreased the dichroism diminishes and we ultimately end up with the PWIA results, e.g. in figure 3 with a single binary peak. The double-peak structure also disappears, i.e. one of the peaks diminishes, when the scattering geometry is chosen far off the condition Im $(ab^*)(\boldsymbol{q}, p_b, \theta_b) = 0 \; \forall \, \theta_b$.

An example is shown in figure 4 both for atomic hydrogen (figure 4(*b*)) and an oriented sodium atom (figure 4(*a*)) for which experimental results are available. At the particular kinematics of figure 4(*b*) one of the peaks, anticipated by the FBA, diminishes to a small subsidiary peak. The origin of this small shoulder is assigned to the double-peak structure, as observed in figure 1. This is deduced by tracing the evolution of the cross section when the geometry is changed from that in figure 1 to figure 4 (results not shown here for space limitations). An optimistic observer can also identify this shoulder in the experimental data for oriented sodium atoms as shown in figure 4(*a*). Interestingly, the PWIA results, shown in figure 4, also show a double-peak shape. The origin of this structure is however distinctively different from that of the FBA calculations. As the cross section within the PWIA can be related to the electron-momentum (probability) density of the initial bound state we can clearly associate the double-peak structure of the PWIA results in figure 4 with the nodal structure of the initial bound state.

As experimental measurements could be performed when oriented sodium atoms are used as targets, we also performed in this case, calculations beyond the FBA. For this particular target and kinematics we present in figure 4(*a*) calculations employing the DWBA (Madison *et al* 1977, McCarthy 1995). Within the DWBA and when the LS coupling is assumed valid,

the exact unsymmetrized T-matrix elements are approximated, as

$$\langle \boldsymbol{p}_a \boldsymbol{p}_b \Phi^{ion}_{J_i L_i M_i} | T | \Phi^{atom}_{JLM} \boldsymbol{p}_0 \rangle \equiv \langle \chi^{(-)}(\boldsymbol{p}_a) \chi^{(-)}(\boldsymbol{p}_b) | V | \phi_{LM} \chi^{(+)}(\boldsymbol{p}_0) \rangle. \tag{11}$$

In relation (11), ϕ_{LM} is the one-electron orbital of the active target electron, i.e. the electron ejected from the atom during the ionization process. The distorted waves, $\chi^{(\pm)}(\boldsymbol{p}_j)$, $j \in \{0, a, b\}$, are the one-electron solutions of the single-particle channel Hamiltonian. For the details on the calculations of the T-matrix elements (11) within the DWBA we refer to McCarthy (1995) and McCarthy and Weigold (1995).

In the present situation, we performed a DWBA calculation where both the incoming and scattered electrons are described by a distorted wave calculated by considering the scattering in the field of the atom. The slow outgoing electron is described by a distorted wave calculated in the field of the ion. The radial parts of the distorted waves are obtained as solutions of radial equations of the type

$$\left[\frac{\mathrm{d}^2}{\mathrm{d}r^2} - \frac{l(l+1)}{r^2} - 2v(r) + k^2 \right] u_l(r) = 0. \tag{12}$$

If the scattering in the field of the atom is considered (i.e. if distorted waves of the projectile electron in the entrance and exit channel are calculated) we use for $v(r)$ in relation (12) the local static-exchange potential of Furness and McCarthy (1973).

As can be seen in figure 4(*a*), the experimental cross section is particularly well described within this model. This is particularly the case for the shoulder noticed previously. As for the case of a hydrogenic target, further calculations show that, within the DWBA model, the small peak in the experimental cross section can be traced back to a double-peak structure appearing when the kinematics are varied. This clearly suggests that the shoulder observed in the experimental cross section is a second maximum diminished at this particular kinematics. A closer examination of figure 4(*a*) also reveals that, at this particular kinematics, the symmetry of the state-resolved cross sections around the momentum transfer is maintained despite the short-range interactions that are not present in the conventional FBA but are now included in the DWBA (cf equation (12)).

The comparison between the FBA and DWBA calculations shown in figure 4(*a*) indicates that the short-range interactions only modify the kinematics at which the second maximum is present and that similar behaviour of the state resolved cross section should be anticipated for both sodium and hydrogen targets.

To confirm the dynamical effect, as predicted within the FBA for the case of a hydrogenic target, we show in figures 5(*a*)–(*c*) DWBA calculations performed under the same kinematics as in figures 1–3 for sodium atoms. As can be seen from figure 5(*a*), the state-resolved cross sections reveal the double-peak structure as for the case of hydrogenic targets.

For a fixed scattering angle $\theta_a = 18.4^\circ$, the orientational dichroism is clearly marked while the cross sections appear almost symmetric around the momentum transfer $\boldsymbol{q}$. When θ_a increases to a value of 19.2° (figure 5(*b*)) the orientational dichroism diminishes in accord with the analytical predictions. Finally, when the scattering angle, θ_a, is further increased, the dichroism reappears but with a reverse sign in accord with the analysis presented for the hydrogenic target. This set of calculations clearly validates the analysis presented in the previous section for the case of the hydrogen atom and for the Na target. Thus, we can deduce that this behaviour of the dichroism is almost independent of the size of the atomic target considered and consequently of the short range interactions felt by the electrons.

The studies presented here, which started from a relatively simple dynamical model, the FBA, predict kinematical situations where the orientational dichroism vanishes. We used this observation to discuss the behaviour of the state-resolved cross sections and to explain the shape of the measured spectra for a sodium target atom. The predictions of the simple analytical

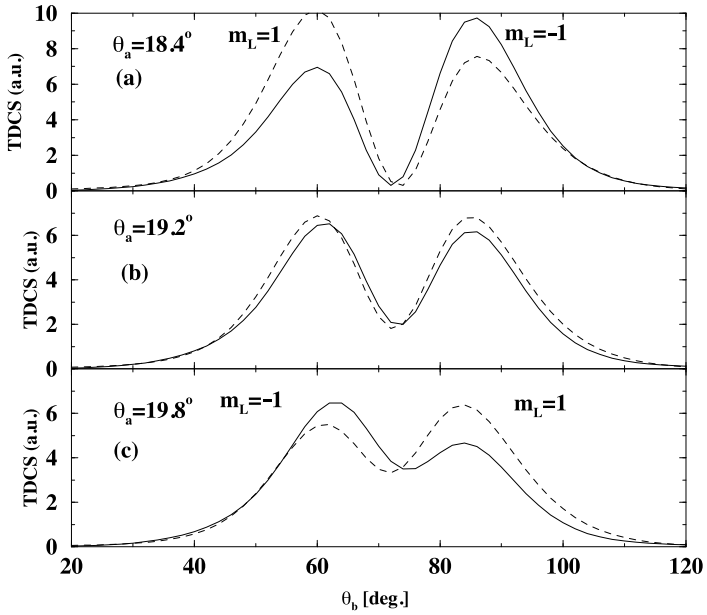

Figure 5. Variation of the initial-state-resolved cross sections as a function of the ejected electron angle, θ_b for three values of the scattered electron angle θ_a (as indicated on the figures) within the DWBA model. The collision geometry is the same as in figure 1 ($E_0 = 150$ eV, $E_b = 10$ eV), however a Na target is used.

model are substantiated by calculations employing a more elaborate theory, the DWBA. This gives more confidence in the accuracy of the anticipated experimental arrangements where the dynamics dictates a vanishing dichroism. An experimental verification of this phenomenon is highly desirable.

Acknowledgments

One of us, SM, wishes to thank the Atomic and Molecular Physics Laboratories at the Australian National University for an invitation during which part of this work was performed and also to acknowledge the financial support from the NSF grant no PHY-9750594.

References

Baum G, Blask W, Freienstein P, Frost L, Hesse S, Rith W, Rappolt P and Streun M 1992 *Phys. Rev. Lett.* **69** 3037

Berakdar J, Engelns A and Klar H 1996 *J. Phys. B: At. Mol. Opt. Phys.* **29** 1109

Dorn A, Elliot A, Guo X, Hurn J, Lower J, Mazevet S, McCarthy I E, Shen Y and Weigold E 1997 *J. Phys. B: At. Mol. Opt. Phys.* **30** 4097

Dorn A, Elliot A, Lower J, Weigold J, Berakdar J, Engelns J and Klar H 1998 *Phys. Rev. Lett.* **80** 257

Ehrhardt H and Röder J 1997 *Coincidence Studies of Electron and Photon Impact Ionization* ed C T Whelan and H R Walters (London: Plenum) p 1

Fehr M, Berakdar J and Klar H 1994 *J. Phys. B: At. Mol. Opt. Phys.* **27** L401

Furness J B and McCarthy I E 1973 *J. Phys. B: At. Mol. Phys.* **6** 2280

Guo X, Lower J, Hurn J, Mazevet S, Shen Y, Weigold E, Granitza B and McCarthy I E 1996 *Phys. Rev. Lett.* **76** 1228

Madison D H, Calhoun R V and Shelton W N 1977 *Phys. Rev.* A **16** 552

McCarthy I E 1995 *Aust. J. Phys.* **48** 1

McCarthy I E and Weigold E 1976 *Phys. Rep.* C **27** 275
——1995 *Electron–Atom Collisions* (Cambridge: Cambridge University Press)
Prinz H Th, Besch K and Nakel W 1995 *Phys. Rev. Lett.* **74** 243